OUKA
Osaka University Knowledge Archive

Title	Picosecond ultrasound spectroscopy for studying elastic modulus of thin films: A review
Author(s)	Ogi, Hirotsugu; Nakamura, Nobutomo; Hirao, Masahiko
Citation	Nondestructive Testing and Evaluation. 2011, 26(3-4), p. 267-280
Version Type	AM
URL	https://hdl.handle.net/11094/84473
rights	
Note	

Osaka University Knowledge Archive : OUKA

https://ir.library.osaka-u.ac.jp/

Osaka University

Picosecond Ultrasound Spectroscopy for Studying Elastic Modulus of Thin Films: A Review

Hirotsugu Ogi, Nobutomo Nakamura, and Masahiko Hirao

Graduate School of Engineering Science, Osaka University
Toyonaka, Osaka 560-8531, Japan

Corresponding Author: Hirotsugu Ogi (ogi@me.es.osaka-u.ac.jp)

Picosecond Ultrasound Spectroscopy for Studying Elastic Modulus of Thin Films: A Review

This paper introduces an advanced acoustic method for measuring the out-of-plane longitudinal-wave modulus of thin films using picosecond ultrasound. The ultrafast light pulse is focused on the film surface to excite the coherent acoustic pulse, which propagates in the thickness direction, and then the time delayed probing light pulse irradiates the specimen for detecting the acoustic waves. For opaque thin films, the pulse echoes within the film or the thickness resonance frequency of the film is measured to determine the modulus. For transparent films, Brillouin oscillations from the film are observed, and their frequencies yield the modulus. The film thickness and refractive index are measured by x-ray reflectivity and ellipsometry, respectively. This method was applied to various thin films, providing important knowledge about the elasticity of thin films. Most thin films are softer than corresponding bulk materials, but some thin films are significantly stiffer.

Keywords: elastic constants, thin films, picoseconds ultrasound, x-ray reflectivity, ellipsometry

Introduction

The elastic stiffness is a fundamental mechanical property, reflecting the interatomic potential of the lattice. Practically, it is a key parameter in designing acoustic resonator devices. Scientifically, it is interesting to investigate the change in the elastic stiffness in ultrathin films, where significant influence of the surface effect is expected. Furthermore, it macroscopically involves defect information because high stress field near defects causes larger deformation locally, reducing the averaged stiffness. Measuring elastic constants then allow us to evaluate defect and inclusions inside the material non-destructively [1-3]. Thus, the measurement of the elastic constants of thin films remains a central issue in nanotechnology and nanosciences.

Several methods have been presented previously for determining the thin film stiffness, including microtensile test [4-6], microbending test [7, 8], nanoindentation [9, 10], cantilever-vibration method [11, 12], Brillouin-scattering method [13-15], surface-acoustic-wave method [16, 17], and resonant ultrasound spectroscopy [18-21]. These previous methods include several difficulties in determining the elastic

constants of thin films. First, static methods are highly affected by errors in dimensions, especially by the film-thickness error. For example, the microbending test evaluates the in-plane Young's modulus of a thin film using a cantilever-shape specimen from the applied force and resultant deflection at the free end of the cantilever. However, the deflection is proportional to the third power of the film thickness and to the width of the cantilever. Thus, the dimension errors have large influence on the resultant stiffness. Also, many previous methods are strongly affected by the gripping condition: For example, in the microbending method and flexural-vibration method, the maximum bending stress appears at the fixed end and the measurements are significantly affected by the gripping condition, because these methods use a simple beam-bending theory, which assumes a completely fixed (rigid) boundary. In the microtensile test, it is difficult to apply a uniaxial stress in the in-plane direction, and bending and torsional stresses arise as well, affecting the stress-strain relationship significantly. In the dynamic methods, such difficulties are less remarkable, but they are largely affected by the mechanical properties of the substrate under the thin film. In the resonant-ultrasound spectroscopy method, the contribution of the thin film elastic constant to the resonance frequency is significantly smaller, and it cannot be applicable to ultrathin films.

For the thin film modulus, we have proposed picosecond ultrasound spectroscopy coupled with x-ray reflectivity measurement for thickness and with ellipsometry for refractive index of the specimen [22-25]. The ultrafast light pump pulse induces coherent acoustic phonons inside the thin film, which are detected by the delayed probe light pulse. For opaque thin films, the longitudinal-wave stiffness can be obtained either from the pulse echo signals of the coherent acoustic pulse or the Γ-point phonon resonance frequencies. The thin film thickness is needed in this

case, and it can be determined by the x-ray total reflectivity measurement within 5% error. For transparent thin films, the stiffness can be obtained by the Brillouin-oscillation frequency. In this case, the refractive index of the thin film for the probing light is needed, and this can be determined accurately by the ellipsometry measurement. In this review article, we explain the principle of the stiffness determination by the picosecond ultrasound spectroscopy and show some measurements of thin film stiffness.

Concerning the mass density of the thin film, it can be evaluated by the x-ray diffraction (XRD) measurement. In the defective specimens, the mass density will decrease, but its contribution to the sound velocity is much lower than that of the stiffness decrease due to the defects.

Picosecond Ultrasound for Elastic Constant of Thin Films

Thomsen *et al*. [26, 27] have detected high-frequency coherent acoustic phonons using ultrafast pump-probe light pulses for the first time, called picosecond ultrasound. This method is actually powerful, because it allows us to detect the acoustic-wave signals even for ultrathin film thinner than 10 nm.

The stiffness measurement of thin films with picosecond ultrasound falls into three methods. First is the pulse-echo method [24, 27-31], where the coherent acoustic pulse generated by the pump light pulse repeats reflections between the film surface and the film-substrate interface. The round-trip time Δt was measured to determine the sound velocity v. The out-of-plane stiffness $C_\perp$ is then determined by

$$C_\perp = \rho\left(\frac{2d}{\Delta t}\right)^2 \quad (1)$$

Here ρ and d denote the mass density and thickness of the film, respectively. Figure 1 shows schematic of the pulse-echo measurement and an example of pulse echoes observed in a 70-nm Pt film deposited on Si substrate.

Second is the phonon-resonance spectroscopy [22-25], where the Γ-point phonon modes were measured to evaluate the elasticity through their resonance frequencies. Irradiation of the thin film with the ultrafast light pulse (~ 100 fs) induces high-frequency acoustic phonons inside thin films. Most of them disappear quickly because of their incoherence, but the zero-wavenumber phonons about the in-plane direction (Γ-point phonons) remain to produce the standing waves [32, 33]. This is equivalent to the one-dimensional through-thickness resonance, because the diameter of the excitation area by the pumping laser beam (~ 50 μm) is much larger than the film thickness (~ 50 nm). Thus, the out-of-plane stiffness can be determined by

$$C_{\perp} = \rho\left(\frac{2df_p}{p}\right)^2 . \qquad (2)$$

Here f_p denotes the p-th resonance frequency, and p represents the order of the resonance. Figure 2 shows the schematic of the phonon resonance and an example of the measurement for a Pt/Co superlattice thin film on a glass substrate (the total thickness of the film is 28 nm).

Third is the Brillouin-oscillation method [27, 34-38], which arises from interference between the light reflected at the specimen and the light refracted by the acoustic wave propagating in the transparent or translucent material. Figure 3 shows the schematic of the Brillouin-oscillation method and a measurement for an amorphous SiO_2 (a-SiO_2) thin film deposited on a Si substrate. In this measurement, we usually deposit a 10-nm Al film on the specimen surface to launch the high-

frequency acoustic pulse toward the substrate using the thermal expansion of aluminium caused by the pump light pulse. The delayed probe light pulse is partially reflected at the Al surface, penetrates into the specimen, and is partially refracted by the propagating acoustic pulse because of the optoelastic effect. The diffracted light interferes in the surface reflected light, and the total reflectivity of the probe light ΔR oscillates during the propagation of the acoustic wave. In the first-order approximation for strain, the oscillation frequency f_{BO} relates with the sound velocity v via (Bragg's condition) [34]

$$f_{BO} = \frac{2nv}{\lambda_{op}}. \tag{3}$$

Here, n denotes the refractive index of the thin film for the probe light, and λ_{op} is the wavelength of the probe light in vacuum. In Fig. 3, we have f_{BO}=45 and 235 GHz from a-SiO_2 and Si substrate, respectively. This difference is mainly caused by much large refractive index of Si at 400 nm (n=5.57) than that of a-SiO_2 (n=1.48). The high attenuation of the oscillation in Si is caused by attenuation of the probe light, not of the acoustic wave. Figure 4 shows calculated strain pulse generated from Al thin film by the pump light pulse, and its Fourier spectrum. The strain pulse consists of phonons of broad frequency range, and the observable components are selected by the wavelength of the probe light inside the material.

Therefore, we can determine the sound velocity and then the stiffness $C_\perp$ by measuring the Brillouin-oscillation frequency without information of the film thickness. Because this method does not require the back echo of the acoustic wave, it can be applied to a specimen having a single flat face, although it needs the refractive index n at the probing wavelength.

X-ray Reflectivity Measurement for Film Thickness

The pulse-echo method and the phonon resonance method definitely require the thickness of thin film to deduce the elastic constant. This can be made possible using the x-ray reflectivity measurement. The periodic intensity variation appears in the x-ray reflectivity spectrum in the low-angle region, which is caused by interference between x-rays reflected at the film surface and at the film-substrate interface. The period is strongly dependent on the film thickness. The reflectivity coefficient is theoretically calculated as a function of the incidence angle [39], which involves the film thickness as a fitting parameter. A least-squares-fitting procedure is performed to inversely determine the thickness by fitting the theory to the measurement. For example, Figure 5 shows the x-ray diffraction spectrum in a low-angle region observed from a 13.5-nm Pt film deposited on a Si substrate. Many peaks originate from interference between the x ray reflected at the film-substrate interface and that reflected at the film surface. Fitting the multi-reflection theory of x-ray to the measurement, we can extract the film thickness.

Ellipsometry for Refractive Index

The refractive index n of the specimen is needed in determining the elastic constant with the Brillouin-oscillation method. This can be made possible by the ellipsometry method [40]. The ellipsometric angle Ψ was measured as a function of the wavelength between 380 and 1700 nm, and the Lorentz-oscillation model was fitted to extract parameters required for calculating refractive index. Three independent measurements were conducted for three incident angles of 60, 70, and 75 degree for each specimen, and the results were used together in the fitting calculation. Figure 6 shows the typical result for the ellipsometry refractive-index measurement.

The ellipsometric angle predicted by the Lorentz-oscillation model agrees well with the measurement, providing a reliable refractive index as a function of wavelength.

Optics

Figure 7 shows the optics for picosecond ultrasound we developed. A mode-locking titanium-sapphire pulse laser is used for the light sources. Its duration, power, repetition frequency, and wavelength are ~100 fs, ~1 W, and ~80 MHz, and 800 nm. The pulse light is split into two beams by a polarization beam splitter (PBS). The straight-through output of the PBS is reflected by the corner reflector located on a microstage, which changes the light path of the pump pulse. It is then modulated by an acoustic-optic (A/O) modulator with a 100-kHz modulation frequency, and focused on the specimen surface perpendicularly by an objective lens. The pulse-laser power at the specimen surface is 1-20 mW, depending on the tolerance of the specimen. The pump pulse generates the high-frequency coherent phonons in the film. The other output from the PBS is frequency-doubled (400 nm wavelength) by the second-harmonic-generator crystal of β-BaB_2O_4. It is further split into two beams by a beam splitter (BS); one enters the balanced photodetector to produce the reference signal and the other irradiates the specimen surface as the probe pulse to detect the change in the strain caused by coherent acoustic phonons via the photoelastic effect. By changing the path length of the pumping light, the time delay between the pump and probe lights are changed. The output signal of the balanced photodetector enters in a lock-in amplifier to monitor the relative change of the intensity of the reflected probe pulse.

Thin Film Stiffness

Polycrystalline thin films

Figure 8 shows the elastic constant of various metallic thin films measured by the pulse-echo method (d>~50 nm) and the phonon resonance method (d<~50 nm). The vertical axis is normalized by the elastic constants of the corresponding bulk materials, which are predicted by their monocrystal elastic constants and the x-ray diffraction measurement for the grain orientation. Because the thin films are highly textured (closed-packed planes are predominantly parallel to the film surface), we assumed that all the grains are oriented in the same direction. (For example, <111> and <110> directions are in the thickness direction for Pt and Fe, respectively.) Thus, the predicted bulk stiffness is nearly the maximum possible value.

Most thin films show lower stiffness than the bulk values. This is attributed to the defects such as incohesive bonds between grains and vacancies [3, 24], not to the remaining noncrystalline phase. For example, Figure 9 shows the change in the stiffness cause by a post-annealing procedure for Co thin films. The annealing at 500 °C for 30 min decreased the thickness, making the structure denser, and made the crystallinity much better (see the inset). The stiffness increased slightly, but it remains much lower value than the bulk value.

In the case of Cu thin films, the stiffness of as-deposited thin films is lower by 20% than that of the bulk Cu, and it increased up to the bulk value with the annealing process at 200 °C for 30 min [41], while the XRD spectrum remained unchanged, indicating that the defects recovered with the low-temperature annealing process.

Pt is an exception. The stiffness of Pt becomes significantly larger than the bulk value when it is thinner than ~20 nm. Considering that the defects must be included in such ultrathin films more or less, this stiffened structure is surprising. We

measured the out-of-plane strain using the XRD method and estimated the stiffness increase due to the lattice anharmonicity (higher-order elasticity), which could not explain the large increase in the stiffness [22]. Thus, the mechanism of the stiffness increase in ultrathin Pt thin films remains unclear.

Superlattices

The picosecond ultrasound method was adopted for evaluating the elastic constant of superlattice thin films. Clemens and Eesley [42] measured the out-of-plane stiffness of Mo/Ni, Pt/Ni, and Ti/Ni superlattice systems and observed significant softening when the bilayer thickness of the multilayer is smaller than 0.5 nm. Such a softening was significantly observed in Pt/Co superlattices, and strong correlation between the stiffness and the perpendicular magnetic anisotropy in the system [24]. The stiffness anomaly principally arises from unusual interfacial bond strength, and the evaluation of the interfacial elastic stiffness has been a central issue for understanding mechanics of superlattice thin films. Recently, the interfacial stiffness can be evaluated by the picosecond phonon resonance method [43], where two phonon modes, which are sensitive and insensitive to the interface stiffness, are used. The ratio between their resonance frequencies reflects the interface stiffness, while it is nearly independent of the other factors (stiffness, density, and thickness of individual layers, defects and noncrystalline phases inside the layers, and the boundary adhesion with the substrate). The interface elasticity parameter (IEP) is thus defined as the ratio of the resonance frequencies:

$$IEP = \frac{f_2}{2f_1}. \quad (4)$$

Here f_1 and f_2 are the fundamental-mode and second-mode resonance frequencies, respectively. IEP becomes larger as the interlayer stiffness increases and equals 1 for a uniform monolayer. The IEP value was investigated in detail for five layers

superlattices consisting of Pt matrix layers and Co, Fe, and Pd ultrathin interlayers as shown in Fig. 10. The absolute value of the stress of the second mode takes the maxima at the interlayers, which are larger than the stresses at the interlayers of the fundamental mode by a factor 3. Therefore, the elastic constant near the interface affects the second-mode resonance frequency more efficiently than the fundamental-mode. Figure 11 shows examples of the measured phonon resonant vibrations and their FFT spectra for superlattices including Co and Fe ultrathin interlayers. Compared with the Co interlayer case, the superlattice including Fe interlayers shows lower f_2. Thus, the IEP value for Fe interlayer is smaller than that of Co interlayer. (In the case of Fig. 11, the stiffness of the Fe interlayer is only 20% of the stiffness of bulk Fe.) Among various interlayer materials, Co layers showed larger IEP values, indicating that the softening of interface is principally caused by defects such as interfacial dislocations and incohesive atomic bonds, not by the strain, because Co layer bonds with Pt layer coherently and is strained significantly.

Amorphous SiO_2 Thin Films

Amorphous SiO_2 (a-SiO_2) thin film shows positive temperature dependences of the elastic constants C_{ij}, and it has been used for compensating negative temperature dependences of C_{ij} of piezoelectric materials to achieve the temperature-insensitive resonators. Recently, it allows development of high-frequency resonators with a Bragg reflector because of low acoustic impedance and low damping at high frequencies [44, 45]. Therefore, measurement of the acoustic properties of a-SiO_2 thin films has attracted many researchers. Picosecond ultrasound has been adopted for this purpose. Zhu *et al.* [29] studied the frequency dependence of the longitudinal-

wave attenuation of a-SiO_2 thin films up to 440 GHz using the picosecond pulse-echo method. Emery and Devos [35] reported attenuation evaluation of a-SiO_2 thin films at frequencies near 250 GHz using Brillouin oscillations.

Brillouin oscillation with the ellipsometry is a powerful tool for evaluating the stiffness of transparent thin films, and it was applied to determine the stiffness of a-SiO_2. Figure 12 shows Brillouin oscillations for a-SiO_2 thin films deposited on Si substrate using the DC reactive sputtering [38]. The coherent acoustic pulse generated from the Al ultrathin film on the specimen propagates in the thickness direction and causes Brillouin oscillation with the frequency given in Eq. (3). When the acoustic pulse reaches the Si substrate, the high-frequency Brillouin oscillation appears because of the high refractive index of Si at 400 nm. In thin films thinner than 300 nm, a large error appears in the determination of the Brillouin-oscillation frequency because of smaller cycle numbers in the thin film region as shown in the 250-nm a-SiO_2 film in Fig. 12. However, when the film thickness is larger than 400 nm, the error in the resultant stiffness was less than 1%. Figure 13 shows the elastic constant of a-SiO_2 thin film deposited with various sputtering voltage. They show larger elastic constant than the bulk value by up to 16%. This stiffness increase is attributed to the decrease of the Si-O-Si bridging angle and the reduction of the number of the membered ring to cause dense structure. Thus, the stiffness of individual components of acoustic devices has to be measured accurately, and their bulk values should not be used.

Summary

This review emphasises that the picosecond ultrasound spectroscopy is a very important tool for evaluating the stiffness of thin films. It is a nonconcacting method

and free from ambiguity due to the specimen gripping conditions. It requires only a single parameter, the thickness or the refractive index, to determine the sound velocity. The former can be measured by the x-ray reflectivity measurement and the latter is obtained with ellipsometry accurately. Because the thin film stiffness is normally different from the corresponding bulk values, the stiffness of individual components should be accurately measured in designing acoustic devices.

References

1. M. L. Dunn, H. Ledbetter, P. R. Heyliger, C. S. Choi, *Elastic constants of textured short-fiber composites*, J. Mech. Phys. Sol. 44 (1996), pp. 1509-1513.
2. T. Morishita and M. Hirao, *Creep damage modeling based on ultrasonic velocities in copper*, Int. J. Sol. Struc. 34 (1997) pp. 1169-1173.
3. H. Ogi, G. Shimoike, M. hirao, K. Takashima, and Y. Higo, *Anisotropic elastic-stiffness coefficients of an amorphous Ni-P film*, J. Appl. Phys. 91 (2002), pp. 4857-4862.
4. WD Nix, *Mechanical properties of thin films*, Metall. Trans., 20A (1989) pp. 2217-2245.
5. W. Suwito, D. Martin, S. Cunningham, and D. Read, *Elastic moduli, strength, and fracture initiation at sharp notches in etched single crystal silicon microstructures,* J. Appl. Phys. 85 (1999) pp. 3519-3534.
6. H. Huang and F. Spaepen, *Tensile testing of free-standing Cu, Ag and Al thin films and Ag/Cu multilayers*, Acta Mater. 48 (2000) pp. 3261-3269
7. A. Ogura, R. Tarumi, M. Shimojo, K. Takashima and Y. Higo, *Control of Nanocrystalline Orientation Using the Application os a Stress Field in an Amorphous Alloy*, Appl. Phys. Lett. 79 (2001) pp.1042-1044.
8. K. Takashima, S. Koyama, K. Nakai and Y. Higo, *Development of Fatigue Pre-Cracking Method into Micro-Sized Specimens for Measuring Fracture Toughness*, MRS Symp. Proc., 741 (2003) pp. 35-40.
9. N. M. Jennett, A.-S. G, and A. S. Maxwell, *Validated measurement of Young's modulus, Poisson ratio, and thickness for thin coatings by combining instrumented nanoindentation and acoustical measurements*, J. Mater. Res. 19 (2004) pp. 143-148.
10. J. V. Fernandes, J. M. Antunes, N. A. Sakharova, M. C. Oliveira, L. F. Menezes, Young's modulus of thin films using depth-sensing indentation, Phil. Mag. Lett. 90 (2010) pp. 9-22.
11. H. Mizubayashi, J. Matsuno, and H. Tanimoto, *Young's modulus of silver films*, Scripta Mater. 41 (1999) pp. 443-448.
12. S. Sakai, H. Tanimoto, and H. Mizubayashi, *Mechanical behavior of high-density nanocrystalline gold prepared by gas deposition method*, Acta Mater. 47 (1999) 211-217.
13. N. Rowell and G. Stegeman, *Theory of Brillouin scattering from opaque media*, Phys. Rev. B 18 (1978) pp. 2598-2615.
14. A. Moretti, W. Robertson, B. Fisher, and R. Bray, *Surface-enhanced Brillouin scattering on silver films*, Phys. Rev. B 31 (1985) pp. 3361-3368.
15. J. Sandercock, in Light Scattering in Solids III, edited by M.Cardona and G. Güntherodt, Topics in Applied Physics Vol. 51 (Springer, New York, 1982), p. 173.
16. A. Moreau, J. Ketterson, and J. Huang, *Three methods for measuring the ultrasonic velocity in thin films*, Mater. Sci. Eng. A 126 (1990) pp. 149-154.
17. J. Kim, J. Achenbach, M. Shinn, and S. Barnett, *Effective elastic constants and acoustic properties of single-crystal TiN/NbN superlattices*, J. Mater. Res. 7 (1992) pp. 2248-2256.
18. J. H. So, J. R. Gladden, Y. F. Hu, J. D. Maynard, and Qi Li, *Measurements of Elastic Constants in Thin Films of Colossal Magnetoresistance Material*, Phys. Rev. Lett. 90 (2003) 036103.

19. H. Ogi, N. Nakamura, H. Tanei, R. Ikeda, M. Hirao, and Mikio Takemoto, *Off-diagonal elastic constant and sp^2-bonded graphitic grain boundary in nanocrystalline-diamond thin films*, Appl. Phys. Lett. 86 (2005) 231904.
20. N. Nakamura, H. Ogi, T. Ono, and M. Hirao, *Elastic constants and magnetic anisotropy of Co/Pt superlattice thin films*, Appl. Phys. Lett. 86 (2005) 111918.
21. K. A. Pestka, II, J. D. Maynard, D. Gao, and C. Carraro, *Measurement of the Elastic Constants of a Columnar SiC Thin Film*, Phys. Rev. Lett. 100, (2008) 055503.
22. H. Ogi, M. Fujii, N. Nakamura, T. Yasui, and M. Hirao, *Stiffened ultrathin Pt films confirmed by acoustic-phonon resonances*, Phys. Rev. Lett. 98 (2007) 195503.
23. H. Ogi, M. Fujii, N. Nakamura, T. Shagawa, and M. Hirao, *Resonance acoustic-phonon spectroscopy for studying elasticity of ultrathin films*, Appl. Phys. Lett. 90 (2007) 191906.
24. N. Nakamura, H. Ogi, T. Yasui, M. Fujii, and M. Hirao, *Mechanism of Elastic Softening Behavior in Superlattice*, Phys. Rev. Lett. 99 (2007) 035502 (2007).
25. H. Tanei, N. Nakamura, H. Ogi, M. Hirao, R. Ikeda, *Unusual elastic behavior of nanocrystalline diamond thin films*, Phys. Rev. Lett. 100 (2008) 016804.
26. C. Thomsen, J. Strait, Z. Vardeny, H. J. Maris, J. Tauc, and J. J. Hauser, *Coherent Phonon Generation and Detection by Picosecond Light Pulses*, Phys. Rev. Lett. 53 (1984) 989-992.
27. C. Thomsen, H. T. Grahn, H. J. Maris, and J. Tauc, *Surface generation and detection of phonons by picosecond light pulses*, Phys. Rev. B 34 (1986) pp. 4129-4138.
28. H. T. Grahn, H. J. Maris, J. Tauc, and K. S. Hatton, *Elastic properties of silicon oxynitride films determined by picosecond acoustics*, Appl. Phys. Lett. 53 (1988) pp. 2281-2283.
29. T. C. Zhu, H. J. Maris, and J. Tauc, Attenuation of longitudinal-acoustic phonons in amorphous SiO_2 at frequencies up to 440 GHz, Phys. Rev. B 44 (1991) pp. 4281-4289.
30. A. Devos and C. Lerouge, *Evidence of Laser-Wavelength Effect in Picosecond Ultrasonics: Possible Connection With Interband Transitions*, Phys. Rev. Lett. 86 (2001), 2669-2672.
31. O. B. Wright, B. Perrin, O. Matsuda, and V. E. Gusev, *Ultrafast carrier diffusion in gallium arsenide probed with picosecond acoustic pulses*, Phys. Rev. B 64, 081202(R).
32. H. Tanei, K. Kusakabe, H. Ogi, N. Nakamura, and M. Hirao, *Observation of gamma-point phonon frequency in ultrathin metallic films confirmed by ab initio calculation and lattice dynamics*, Appl. Phys. Lett. 95 (2009) 011902.
33. K. Tanigaki, T. Kusumoto, H. Ogi, N. Nakamura, M. Hirao, *Measurement of Elastic Constant and Refraction Index of Thin Films at Low Temperatures Using Picosecond Ultrasound*, Jpn. J. Appl. Phys. 49 (2010) 07HB01.
34. A. Devos and R. Côte, *Strong oscillations detected by picosecond ultrasonics in silicon:Evidence for an electronic-structure effect*, Phys. Rev. B 70 (2004) 125208.
35. P. Emery and A. Devos, *Acoustic attenuation measurements in transparent materials in the hypersonic range by picosecond ultrasonics*, Appl. Phys. Lett. 89 (2006) 191904.
36. A. Devos, M. Foret, S. Ayrinhac, P. Emery, and B. Rufflé, *Hypersound damping in vitreous silica measured by picosecond acoustics*, Phys. Rev. B 77 (2008), 100201(R).

37. O. Matsuda, O. B. Wright, D. H. Hurley, V. E. Gusev, and K. Shimizu, *Coherent Shear Phonon Generation and Detection with Ultrashort Optical Pulses*, Phys. Rev. Lett. 93 (2004) 095501.
38. H. Ogi, T. Shagawa, N. Nakamura, M. Hirao, H. Odaka, N. Kihara, *Elastic constant and Brillouin oscillations in sputtered vitreous SiO2 thin films*, Phys. Rev. B 78 (2008) 134204.
39. L. Parratt, *Surface Studies of Solids by Total Reflection of X-Rays*, Phys. Rev. 95 (1954) 359-369.
40. H. G. Tompkins and W. A. McGahan, *Spectroscopic Ellipsometry and Reflectometry* (Wiley, New York, 1999).
41. N. Nakamura, H. Ogi, and M. Hirao, *Stable Elasticity of Epitaxial Cu Thin Films on Si*, Phys. Rev. B 77 (2008) 245416.
42. B. M. Clemens and G. L. Eesley, *Relationship between Interfacial Strain and the Elastic Response of Multilayer Metal Films*, Phys. Rev. Lett. 61 (1988) 2356-2359.
43. H. Ogi, T. Shagawa, N. Nakamura, and M. Hirao, *Extraction of Interface Stiffness in Superlattices: Proposal of the Interface Elasticity Parameter*, Appl. Phys. Express 2 (2009) 105001.
44. S. Rabaste, J. Bellessa, A. Brioudea, C. Bovier, J. C. Plenet, R. Breniera, O. Marty, J. Mugnier, and J. Dumas, *Sol–gel fabrication of thick multilayers applied to Bragg reflectors and microcavities*, Thin Solid Films 416 (2002) pp. 242-247.
45. S. Rey-Mermet, R. Lanz, and P. Muralt, *Bulk acoustic wave resonator operating at 8 GHz for gravimetric sensing of organic films*, Sens. Actuat. B 114 (2006) pp. 681-686.

Figure Captions

Fig. 1 Schematic of the picosecond-ultrasound pulse-echo measurement (upper) and the measured pulse echoes for a 70-nm Pt film deposited on (100) Si substrate (lower). The inset shows the relationship between the arrival time of the acoustic pulse and the number of the pulse *m*.

Fig. 2 Schematic of the picosecond phonon resonance spectroscopy (upper), measured reflectivity change in a28-nm Co/Pt superlattice thin film, and its Fourier spectrum, showing three resonance peaks.

Fig. 3 Schematic of Brillouin oscillation (upper) and the measurement for a 600 nm a-SiO_2 thin film on Si substrate (lower). The low-frequency oscillation (~45 GHz) and high-frequency oscillation (235 GHz) are observed, corresponding to Brillouin oscillation in the a-SiO_2 and the Si substrate, respectively.

Fig. 4 Calculated strain pulse due to the pump-light irradiation (left) and its Fourier spectrum (right).

Fig. 5 X-ray total reflectivity measurement (solid circles) and fitted theoretical function (solid line) for a 13.5-nm Pt on a Si substrate.

Fig. 6 Measured (solid lines) and calculated (broken lines) ellipsometry angles at three incident angles for an a-SiO_2 film on a Si substrate.

Fig. 7 Optics of picosecond ultrasound.

Fig. 8 Thickness dependence of the out-of-plane longitudinal-wave elastic constant $C_\perp$ of various metallic thin films normalized by that of corresponding bulk materials.

Fig. 9 The elastic constant of Co thin films on glass (diamonds) and Si (circles) substrates. Solid marks are for measurements of as-deposited thin films, and open marks are those after annealing at 500 ºC for 30 min. The inset shows the change in the XRD spectrum before and after the annealing process.

Fig. 10 Thickness resonance modes in a five layer superlattice. Solid lines represents the displacement. The fundamental mode (f_1) shows smaller the maximum stress at the interlayer, but the second mode (f_2) shows the maximum stress at the interlayer.

Fig. 11 Reflectivity changes in Pt/Co and Pt/Fe superlattices (left) and their FFT spectra.

Fig. 12 Brillouin oscillations for a-SiO_2/Si specimens.

Fig. 13 Relationship between the elastic constant of a-SiO_2 thin films and the sputtering voltage. The broken line represents the stiffness of a bulk a-SiO_2.

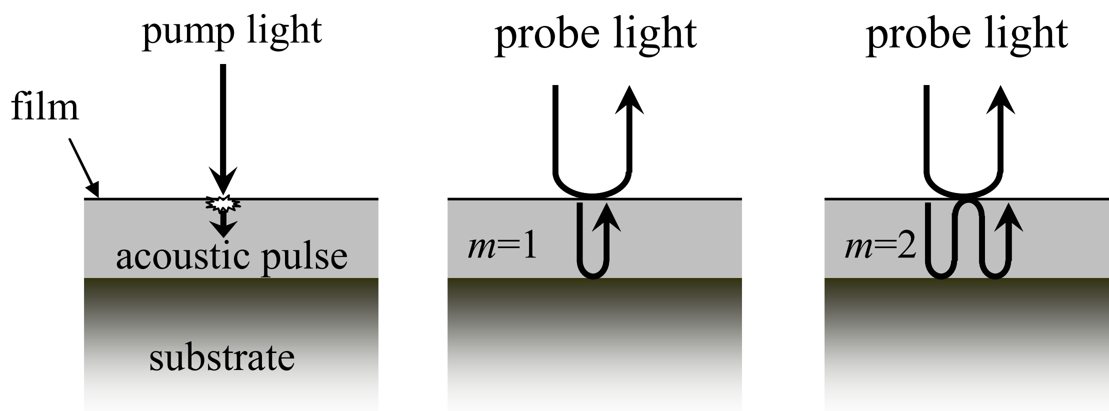

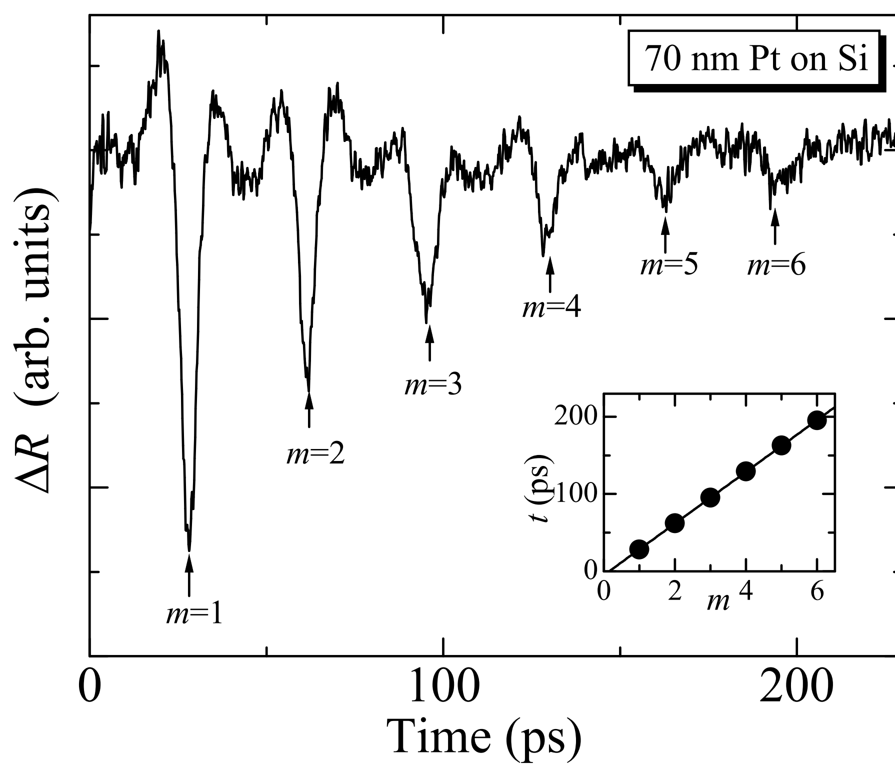

Fig. 1

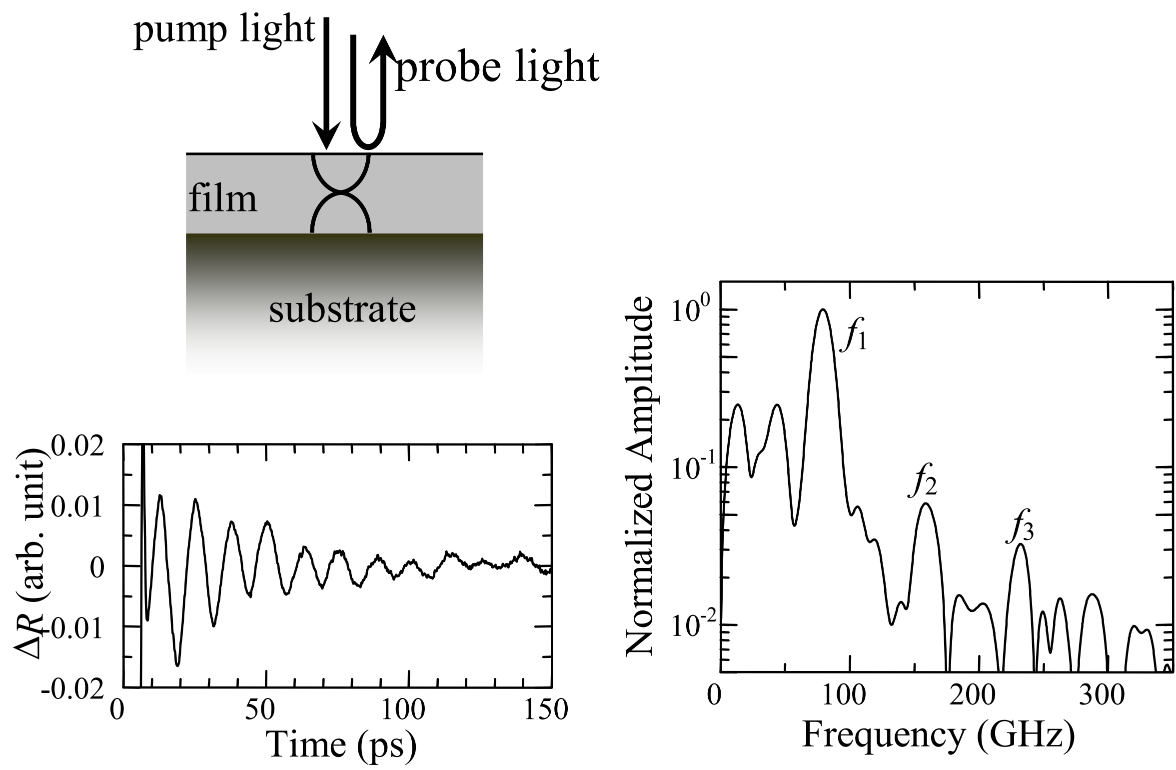

Fig. 2

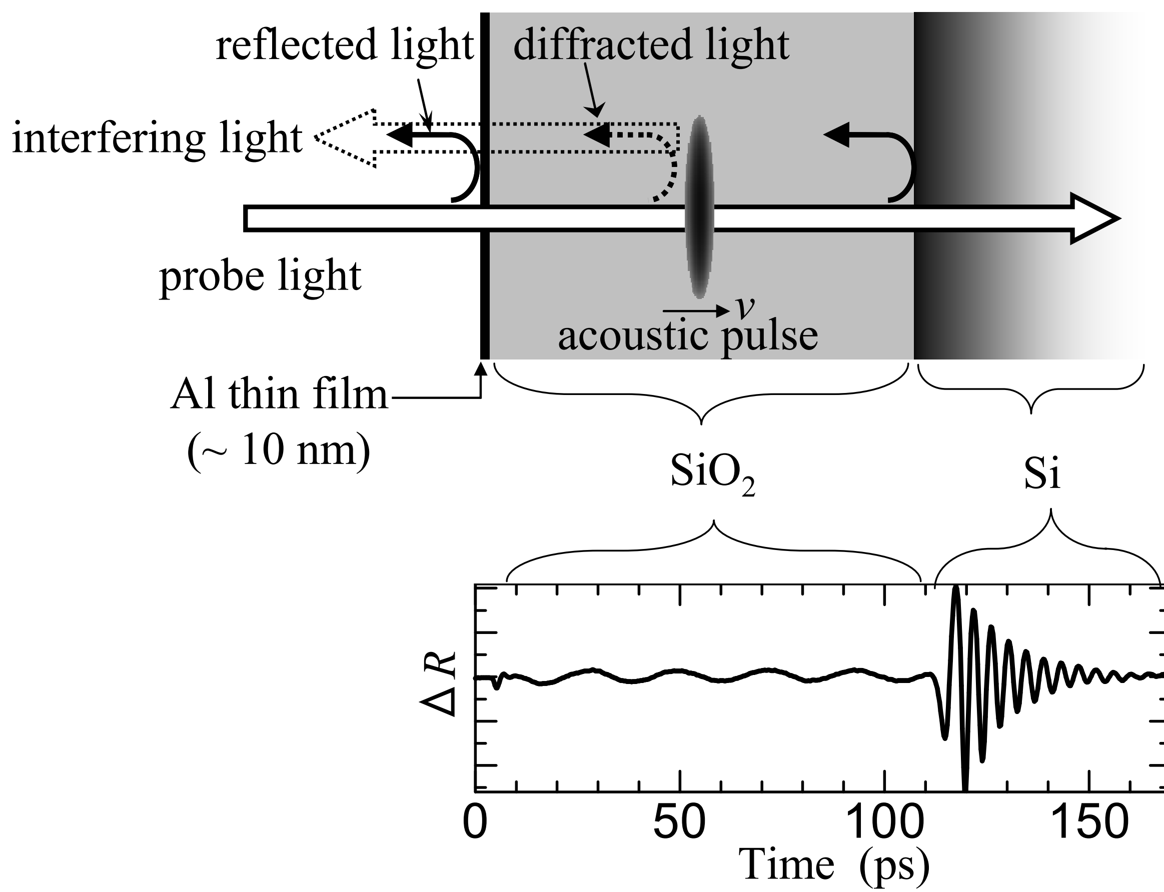

Fig. 3

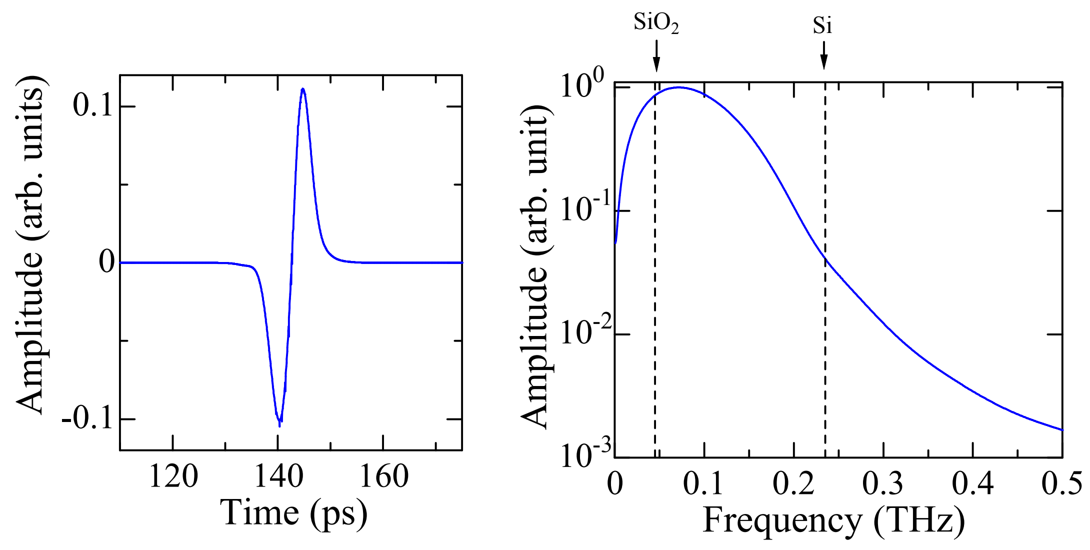

Fig. 4

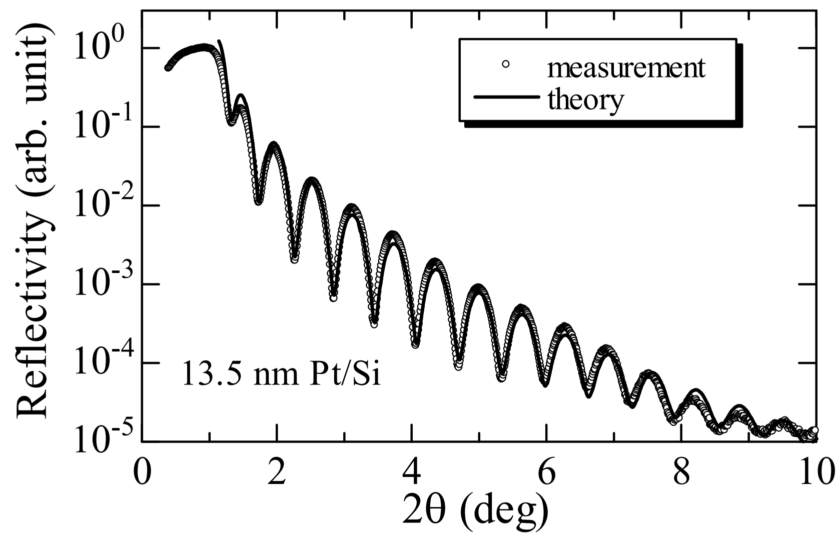

Fig. 5

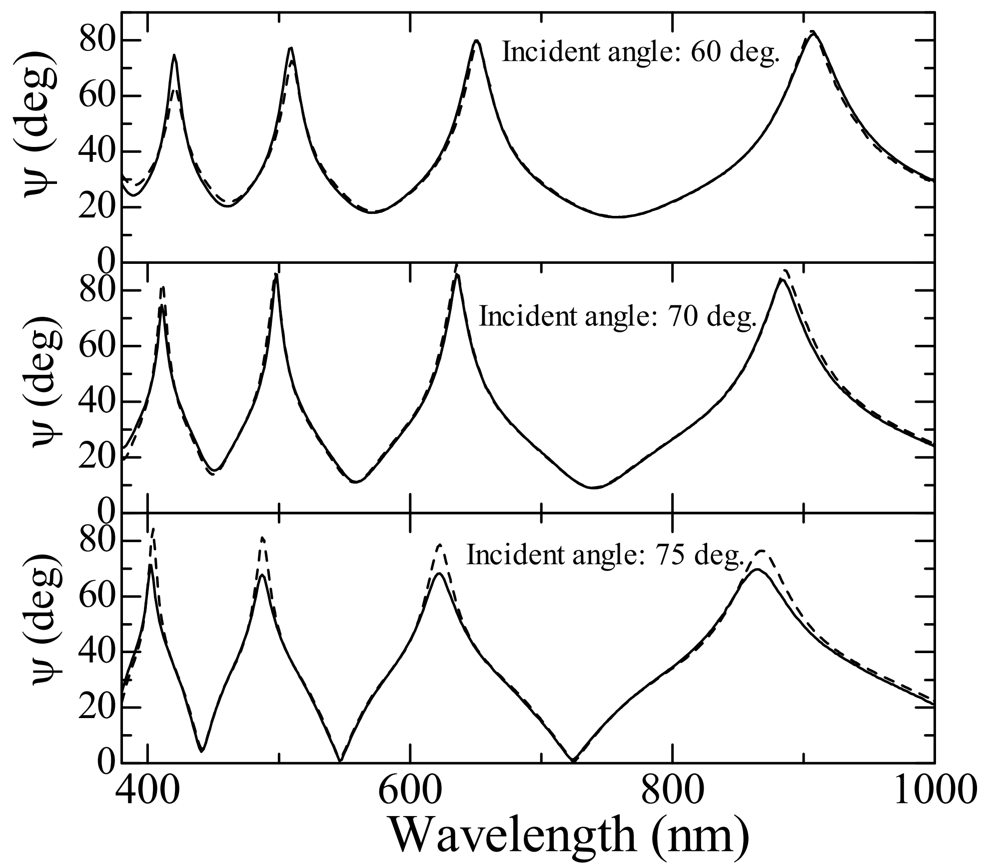

Fig. 6

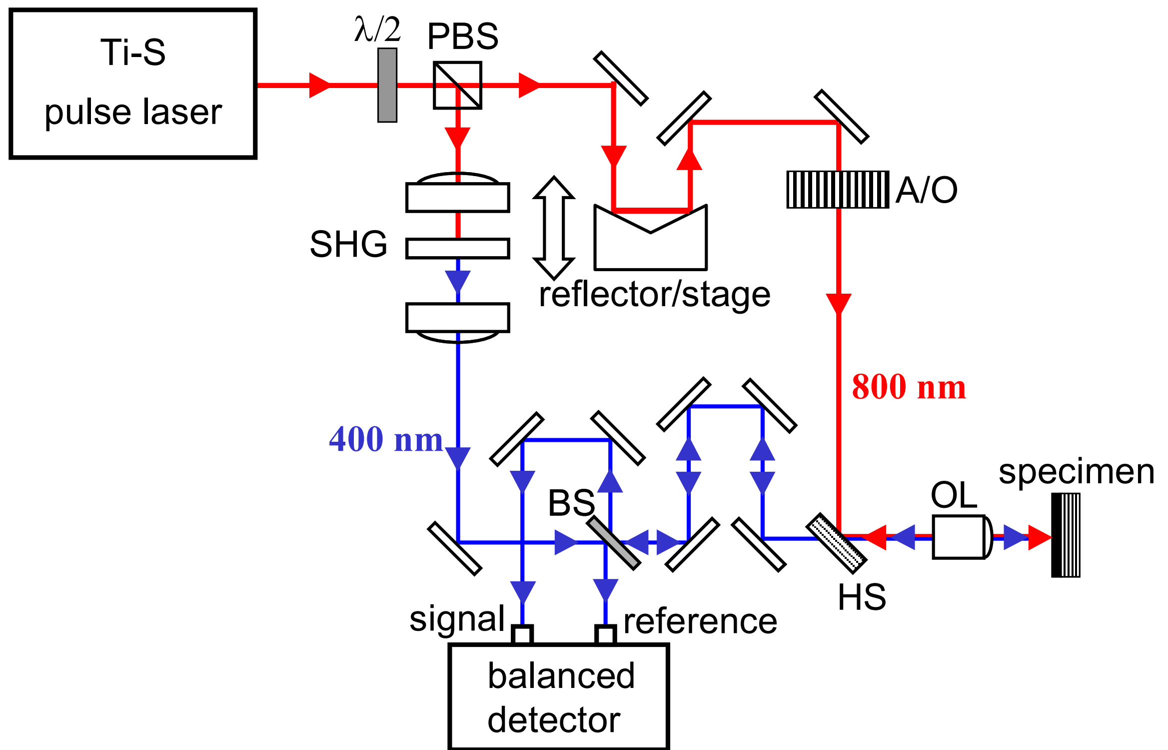

Fig. 7

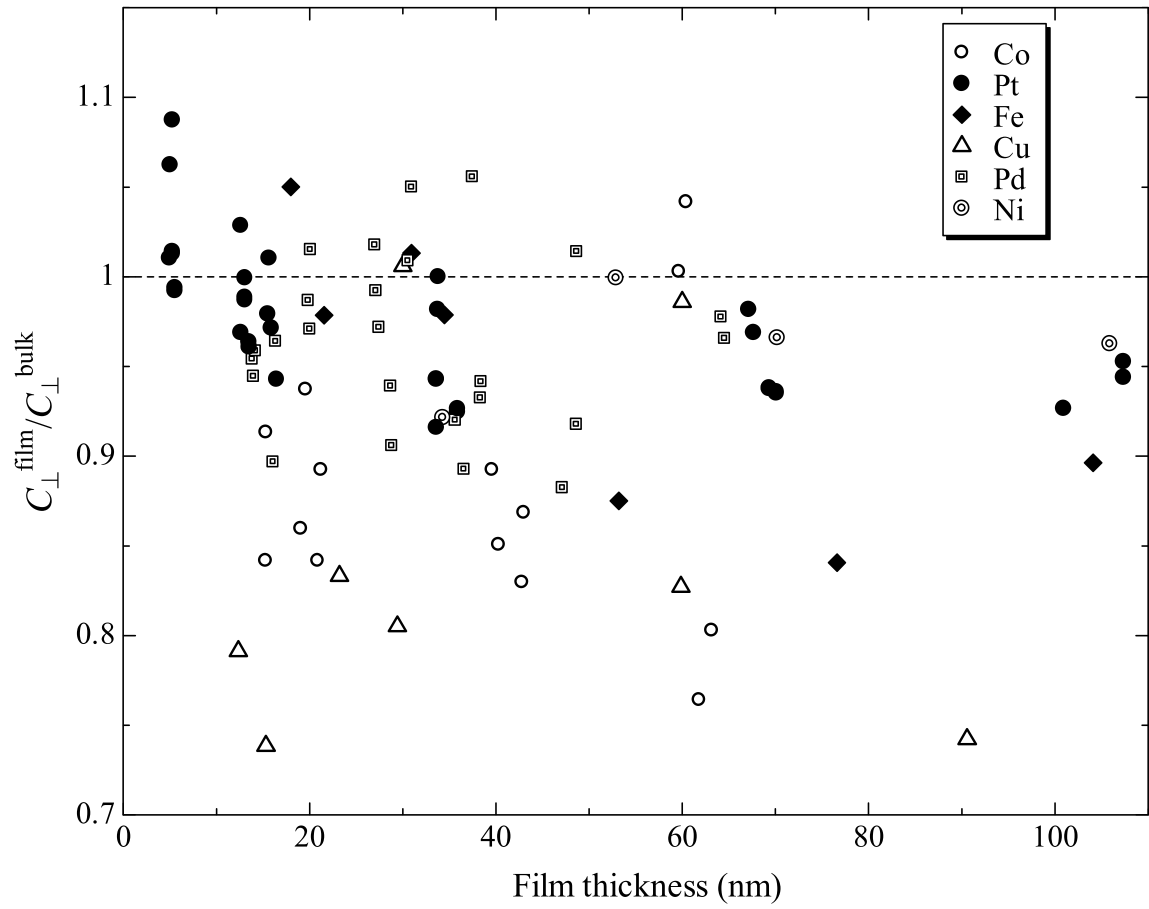

Fig. 8

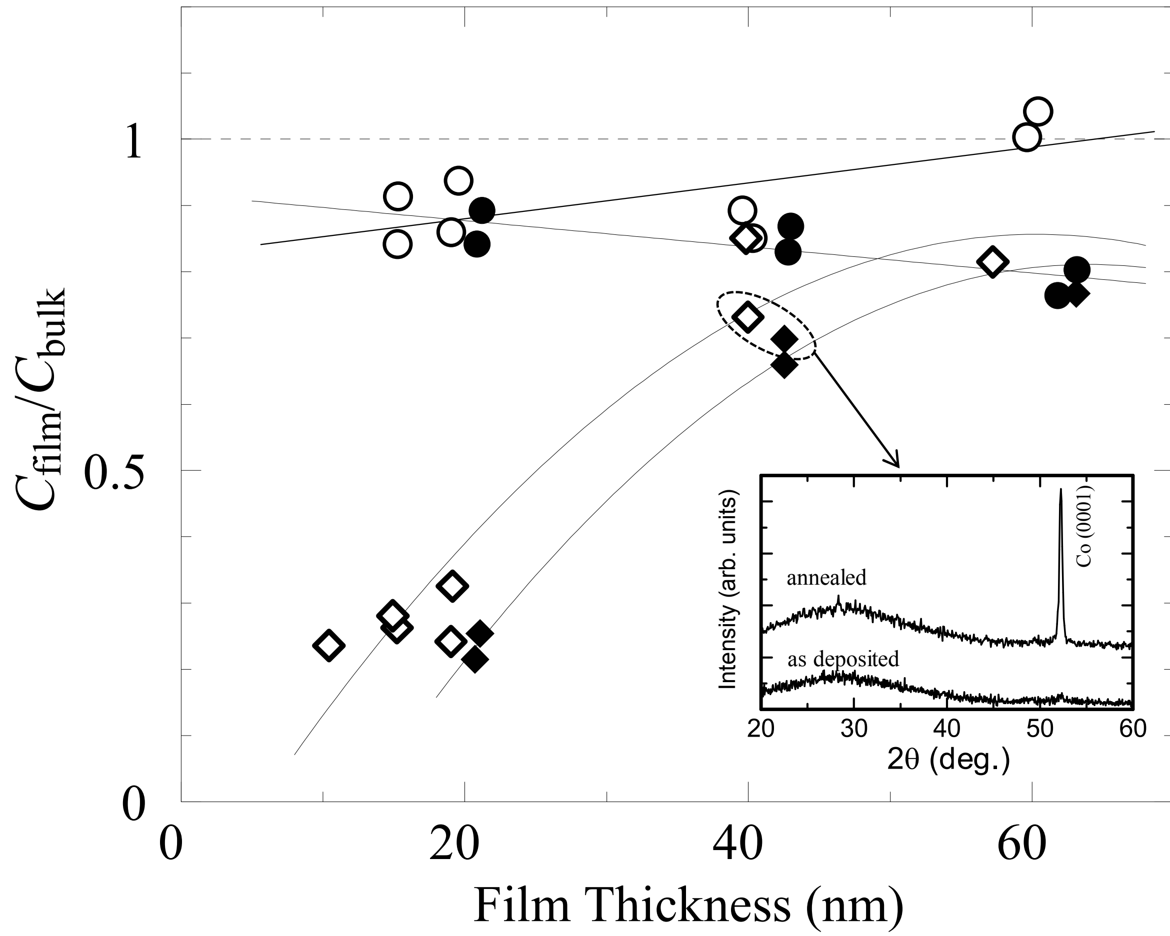

Fig. 9

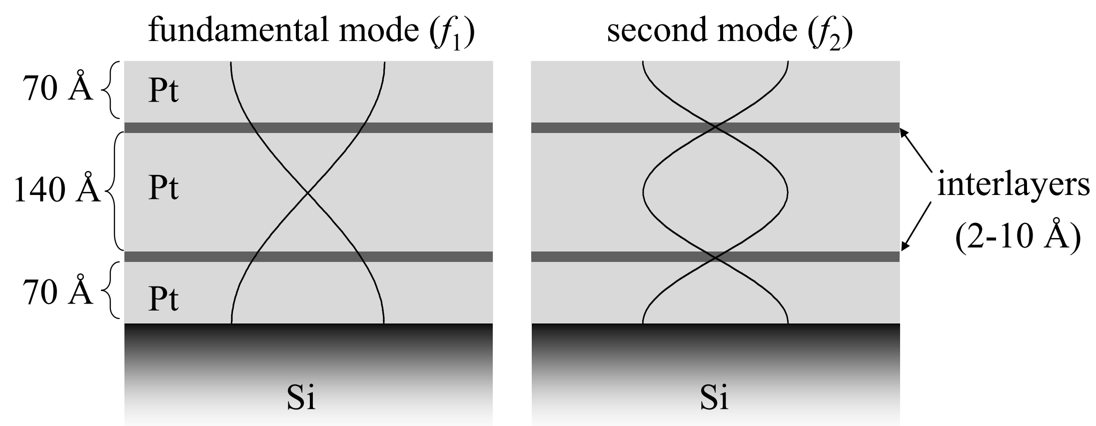

Fig. 10

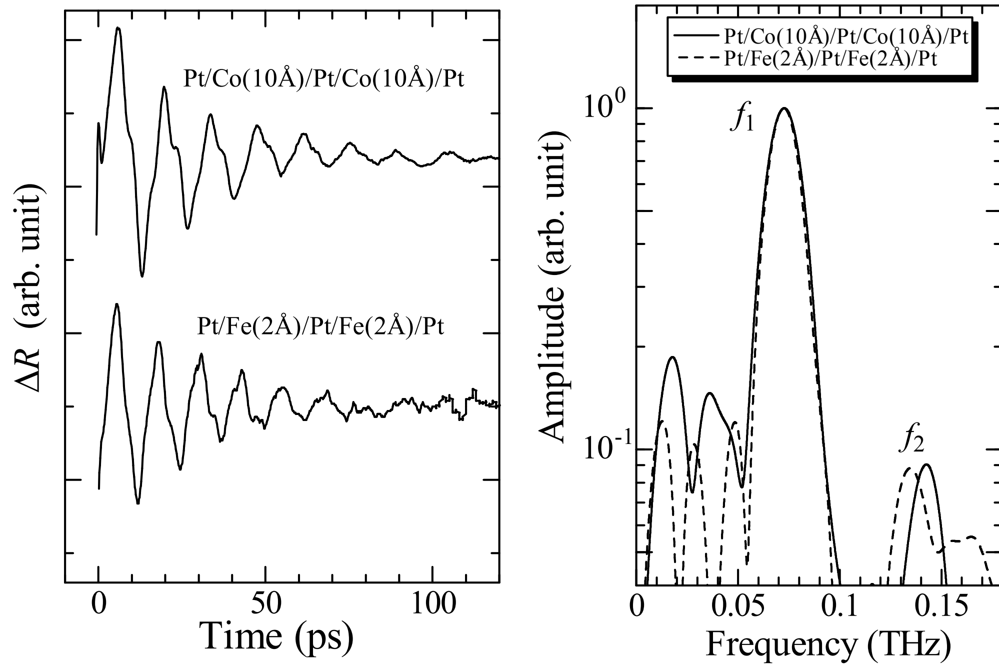

Fig. 11

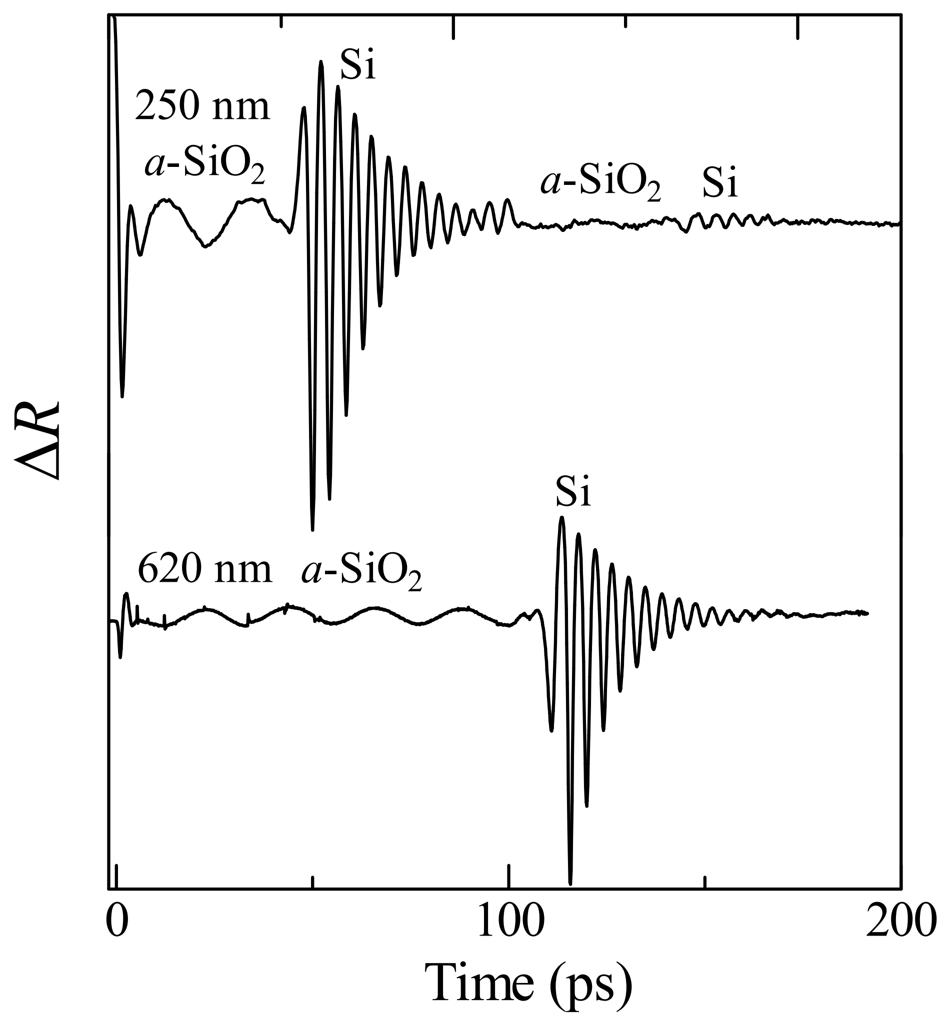

Fig. 12

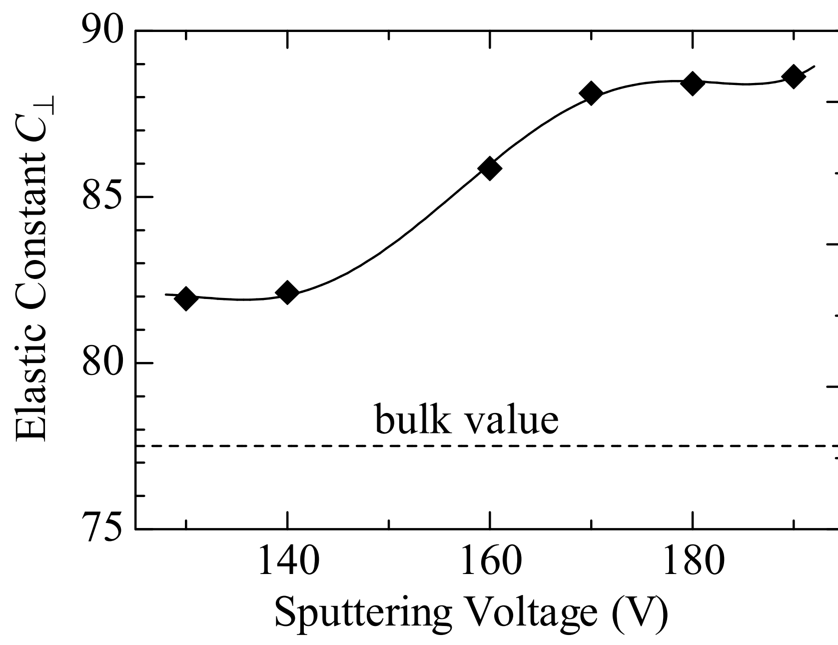

Fig. 13